Diverse Calcium Channel Types are Present in the Human Placental Syncytiotrophoblast Basal Membrane

L. Bernucci, M. Henríquez, P. Díaz, G. Riquelme*

Laboratorio de Electrofisiología de Membranas, Programa de Fisiología y Biofísica, ICBM, Facultad de Medicina, Universidad de Chile, Casilla 70005, Correo 7, Santiago 7, Chile

Abstract

The functional expression of calcium channels has been scarcely studied in human placental syncytiotrophoblast. We have presently sought to characterize Ca^{2+} currents of the healthy syncytiotrophoblast basal membrane using purified basal membranes reconstituted in giant liposomes subjected to patch-clamp recordings.

We detected presence of channels with high permeability to Ca^{2+} (relative PCa/PK up to 99.5) using K^+ solutions in symmetric conditions. Recordings performed in Ba^{2+} gradients showed Ba^{2+}-conducting channels in 100% of experiments. Ba^{2+} total patch currents were consistently blocked by addition of $NiCl_2$, Nifedipine (L-type voltage-gated calcium channel blocker) or Ruthenium Red (TRPV5−TRPV6 channel blocker); Nifedipine and Ruthenium Red exerted a synergic blocking effect on Ba^{2+} total patch currents. Immunohistochemistry of placental villi sections evidenced presence of α_1 subunit of voltage-gated calcium channels and TRPV5−TRPV6 channels in basal and apical syncytiotrophoblast plasma membranes; these three calcium channels were also detected in purified basal and apical fractions using Western blot. These results show the presence of three types of calcium channels in the syncytiotrophoblast basal membrane by both functional and molecular means. These basal membrane calcium channels would not be directly involved in mother-to-fetus Ca^{2+} transport, but could participate in other relevant trophoblast processes, such as exocytosis and Ca^{2+} transport regulation.

Keywords: Placenta; Syncytiotrophoblast; Basal membrane; Calcium channels

1. Introduction

As in all other cell types, Ca^{2+} appears to play a role as a second messenger in the human syncytiotrophoblast. This has been suggested by multiple studies, particularly considering the participation of Ca^{2+} in hormone secretion by cultured trophoblast or placental explants [1−11]. Participation of L-type voltage-gated calcium channels (VGCC) in hormone secretion was studied in eight of the 11 mentioned studies by adding specific blockers (dihydropyridines and phenylalkylamines) to the culture media; in seven of these eight studies blocker addition resulted in suppression of intracellular Ca^{2+} concentration rise and hormone secretion, suggesting participation of these channels in the secretory process. Some studies using placental explants, however, do not suggest the participation of VGCC in hormone secretion [58]. On the other hand, no functional evidence for the presence of VGCC was demonstrated by Ca^{2+} uptake in BeWo cells [12] and using patch-clamp recording [13] or cytofluorimetric analysis [14] in cultured trophoblast cells, leading to a persistent controversy regarding the nature of Ca^{2+} channels in the human trophoblast. More recently, L-type Ca^{2+} channel α_1-subunit expression (α_{1C} and α_{1D}) has been detected using RT-PCR in cultured trophoblast cells [15]. However, as would be expected, it seems that VGCC are not the only Ca^{2+}-conducting channels expressed in trophoblast cells, as expression of several Ca^{2+}-conducting channels from the TRP (Transient Receptor Potential) superfamily has also been recently

* Corresponding author. Tel.: +56 2 9786206; fax: +56 2 7776916.
E-mail address: griquelm@med.uchile.cl (G. Riquelme).

demonstrated using both RT-PCR in cultured trophoblast [15,16], RT-PCR in villous placental tissue and immunohistochemistry of villous placental tissue [17]. TRPV5 and TRPV6 channel plasma membrane activity was suggested by block of basal Ca^{2+} uptake in cultured trophoblast cells when adding magnesium and Ruthenium Red, non-specific blockers for these channels [16]; TRPC channel plasma membrane activity was suggested by block of depletion-activated Ca^{2+} entry in term placental villous fragments when adding gadolinium and SKF96365, non-specific blockers for some TRPC channels [17].

According to the above mentioned studies, candidates for ligand-independent trophoblast Ca^{2+} entry belong to two main families of Ca^{2+} channels: VGCC − particularly L-type VGCC − and TRP channels.

Voltage-gated calcium channels (VGCC) are highly selective for Ca^{2+} over monovalent cations, choosing Ca^{2+} over Na^{+} in spite of their identical diameter (relative PCa/PNa ≈ 1000) [18]. Current nomenclature is based on the pore-forming subunit gene subfamily of the channel (α_1 subunit, subfamilies 1−3: Ca_v1, Ca_v2, Ca_v3) [19], although the first recorded channels were originally named according to the electrophysiological characteristics of their currents [20]: L-type (*l*arge conductance, *l*asting current; presently Ca_v1), T-type (*t*iny conductance, *t*ransient current; presently Ca_v3), N-type (*n*euronal; presently Ca_v2 together with P/Q-type and R-type VGCC). The pharmacology of the three α_1 subunit subfamilies is a useful tool to distinguish among Ca^{2+} currents, as channel blockers are quite specific. For example, the dihydropyridine Nifedipine is a specific blocker for the Ca_v1 (L-type) subfamily [19].

TRP (*T*ransient *R*eceptor *P*otential) ion channel subunit genes were first defined in the Drosophila visual system and named after the transient response of the transmembrane voltage potential of mutant retinal neurons to light in contrast to the sustained response in wild type [21]. Current nomenclature of the TRP superfamily includes three families based on sequence homology and functional similarity: TRPC (Canonical) family, TRPV (Vanilloid receptor) family, and TRPM (Melastatin) family. TRP channels characteristically behave as non-selective cation channels with an equivalent permeability to monovalent cations Na^{+} and K^{+} (relative PNa/PK = 1); they share, however, the property of being permeable to Ca^{2+} with relative PCa/PNa ≤ 10, with the exception of TRPM4 and TRPM5 which are monovalent cation selective, and of TRPV5 (also called ECaC1 or CaT2) and TRPV6 (also called ECaC2 or CaT1) which are highly Ca^{2+}-selective (relative PCa/PNa > 100) [22].

In spite of the compelling evidence for the presence of members of these two families of Ca^{2+}-conducting channels in the syncytiotrophoblast plasma membrane, there are few studies that deal with the electrophysiological characterization of plasma membrane Ca^{2+} currents. Two different non-selective cation channels of the human apical syncytiotrophoblast membrane have been shown to permeate Ca^{2+} [23,24]; one of them (Polycystin-2) belongs to the TRP superfamily. There are presently no equivalent studies in the human syncytiotrophoblast basal membrane, although Ca^{2+} flux measurements of basal membrane vesicles have shown the presence of ATP-independent Ca^{2+} fluxes with channel-like kinetics [25].

The aim of our present work has been to detect Ca^{2+}-conducting channels in the basal syncytiotrophoblast plasma membrane and to study their electrophysiological and pharmacological behavior, according to the current evidence above mentioned. These results will hopefully aid in the understanding of the role of Ca^{2+} as an important signalling factor in the placental epithelium.

2. Materials and methods

2.1. Purification of basal membranes

Purification of basal membranes was achieved using the method described in Jimenez et al. [26], which allows simultaneous isolation of apical and basal membranes from the same placenta, and is based on the method described by Illsley et al. [27] and modified by incorporating steps from our previous protocol for obtaining apical membrane [28] and one step to isolate plasma membrane free of mitochondrial membranes [29].

Placentas obtained from normal term pregnancies were collected immediately after delivery from the San José Hospital Maternity Unit and transported to the laboratory on ice. The purification method involved precipitation of basal membrane with magnesium ions, differential centrifugation and sucrose step gradients. All solutions were buffered with 20 mmol/L Tris−HEPES, pH 7.4. A portion of the basal membrane-enriched preparation containing about 6−8 mg of protein was overlaid on the sucrose gradient. The band at the 47/52% (w/v) sucrose interface was collected and diluted 10-fold with 20 mmol/L Tris−HEPES, pH 7.4, before centrifugation at 110 000 × g for 30 min. The final pellet was resuspended in 300 mmol/L sucrose, 20 mmol/L Tris−maleate, pH 7.4, and stored in liquid nitrogen.

The purity and enrichment of the basal membrane fraction were determined routinely by assaying for classical marker protein activities. Adenylate cyclase and β-adrenergic receptors were used as basal membrane markers, alkaline phosphatase as an apical membrane contamination marker and cytochrome-*c* oxidase/succinate dehydrogenase as mitochondrial membrane contamination markers. Our purified membranes show purity and enrichment parameters comparable to those of other preparations reported for single or paired apical and basal membrane purification (see Jimenez et al. [26]). Because the BM and MVM enrichments are particularly comparable with the method described by Illsley et al. [27], we considered our purified membranes to contain low levels (<12%) of contamination by non-syncytial plasma membranes reported for the isolated membrane fractions. Purified basal membranes were enriched over 9-fold in adenylate cyclase activity relative to the microsomal fraction and 9-fold in dihydroalprenolol binding to β-adrenergic receptors relative to the tissue homogenate, and were essentially free of apical membranes and mitochondrial membranes. Lack of contamination of purified basal membranes with apical membranes and mitochondrial membranes was confirmed using immunoblotting for placental alkaline phosphatase and cytochrome-*c* oxidase, respectively. The densitometric analysis of Western blots (see Fig. 8B) usually gives a relative mark of alkaline phosphatase for pure BM fractions of about 5% of the mark detected in MVM. Accordingly, the enzymatic activity for alkaline phosphatase is also low in BM: enrichment was only 1.5−2-fold relative to the whole tissue homogenates, while the enrichment of alkaline phosphatase activity for MVM fractions is usually in the range of 17−21-fold. The degree of contamination, quantitated by a ratio of alkaline phosphatase activity enrichment of BM compared to MVM (BM/MVM), is 0.15 in our study, lower or equivalent to that from several other reports [26].

2.2. Reconstitution of the purified basal membrane into giant liposomes

Giant liposomes were prepared by submitting a mixture of the reconstituted basal membrane vesicles and asolectin lipid vesicles to a partial

dehydration/rehydration cycle, as reported by Riquelme et al. [30]. A membrane aliquot containing 100−150 μg of protein was mixed with 2 mL of a 13 mmol/L (in terms of lipid phosphorus) suspension of the asolectin vesicles. After the partial dehydration/rehydration cycle, the diameter of the resulting giant multilamellar liposomes ranged from 5 to 100 μm.

2.3. Patch-clamp recordings

Aliquots of 3−6 μL of giant liposomes were deposited into the excised Patch chamber (RC-28, Warner Instruments Corporation, USA) mixed with 0.5 mL of the buffer of choice for electrical recording (bath solution). Single-channel recordings were obtained by patch-clamp techniques as described by Hamill et al. [31]. Giga seals were formed on giant liposomes with glass microelectrodes of 5−10 MΩ resistance. After sealing, withdrawal of the pipette from the liposome surface resulted in an excised patch. Current was recorded with an EPC-9 patch-clamp amplifier (Heka Elektronic, Lambrecht/Pfalzt, Germany) at a gain of 50−100 mV/pA and a filter setting of 10 kHz. The holding potential was applied to the interior of the patch pipette, and the bath was maintained at virtual ground ($V = V_{bath} - V_{pipette}$). The bath was grounded via an agar bridge and the junction potential was compensated for when necessary. The signal was analyzed off-line using TAC (Bruxton Corporation), Pulse Fit (Heka, Lambrecht/Pfalz, Germany) and Microcal Origin 6.0 (Microcal Software, Inc., USA) software. All measurements were made at room temperature.

2.4. Pulse protocols

Three main types of pulse protocols were used in our electrophysiological experiments:

1.- A 40 mV/s voltage ramps from −100 to +100 mV, which allowed measurement of experimental reversal potential (Erev) and of absolute currents generated by brief transmembrane holding voltages. This pulse protocol thus allowed the measurement of isolated Ba^{2+} currents (at $VeqCl^- = -55$ mV) and of isolated Cl^- currents (at $VeqBa^{2+} = +76$ mV) in pipette-to-bath $BaCl_2$ concentration gradient conditions (solution composition 3 in Section 2.5).
2.- Equilibrium potential pulses, consisting of 100 ms holding voltages at the Ba^{2+} theoretical equilibrium potential ($VeqBa^{2+} = +76$ mV) and at the Cl^- theoretical equilibrium potential ($VeqCl^- = -55$ mV) in pipette-to-bath $BaCl_2$ concentration gradient conditions. This pulse protocol also allowed measurement of isolated Ba^{2+} and Cl^- currents.
3.- Increasing voltage pulses, consisting of 5 s holding voltages separated by a 1 s pulse at 0 mV holding voltage, starting at −80 mV and increasing up to +80 mV in steps of 40 mV. This pulse protocol was used only to detect Cl^- channels in solutions of NMDGCl.

2.5. Solutions and blockers

The pipette and bath solutions were prepared with de-ionized water (Ca^{2+} concentration 10 μmol/L, measured using a fluorometric method − Fluoromax ISA Instruments), and had the following composition, according to the experimental strategy that was used (in mmol/L):

1.- Pipette and bath: 135 Kgluconate, 5 KCl, 10 NaHEPES, pH 7.4.
2.- Pipette and bath: 140 NMDGCl (N-methyl-D-glucamine chloride), 10 NaHEPES, 2.5 $CaCl_2$, 1.25 $MgCl_2$, pH 7.4.
3.- Pipette: 40 $BaCl_2$, 10 TrisCl, pH 7.4. Bath: 0.1 $BaCl_2$, 10 TrisCl, pH 7.4.
4.- Pipette: 40 $BaCl_2$, 10 TrisCl, 0.5 DIDS, pH 7.4. Bath: 0.1 $BaCl_2$, 10 TrisCl, 0.5 DIDS, pH 7.4.

Ba^{2+} ions were used as charge carriers for the following reasons. (a) Ba^{2+} ions, unlike Ca^{2+} ions, do not block calcium channels. (b) Ba^{2+} ions usually move through single calcium channels faster than other divalent cations. (c) Ba^{2+} ions block many types of monovalent cation channels that may complicate the single calcium channel current measurements. (d) Ba^{2+} ions, unlike Ca^{2+} ions, do not activate other conductances.

Working blocker solutions were prepared from concentrated stock solutions by dilution with the corresponding experimental bath solution, so as not to change bath conditions. DIDS (4,4′-diisothiocyanatostilbene-2,2′-disulfonic acid) and Nifedipine were dissolved in DMSO (di-methyl-sulphoxide), and calculations were made to reach a maximum DMSO bath concentration of 0.1% when adding 1 mmol/L DIDS or 10 μmol/L Nifedipine to the bath solution. Concentrated solutions of 9.8 and 392 μmol/L of Ruthenium Red in the corresponding working bath solution were used to raise the Ruthenium Red bath concentration to values ranging from 111 nmol/L to 18 μmol/L. Concentrated solutions of 10 and 50 mmol/L $NiCl_2$ were used to raise Ni^{2+} bath concentration to values ranging from 50 nmol/L to 20 mmol/L.

2.6. Immunohistochemistry

Tissue samples from human placenta from normal pregnancies were rinsed in NaCl 0.9% and frozen in cryogel. Ten-micrometer thick sections were fixed with *p*-formaldehyde 4% for 30 min and rinsed three times with TBS buffer (Tris buffered saline, pH 7.6) for 5 min. Sections were blocked overnight with TCT buffer (carrageenan 0.7%, Triton X-100 0.5% in TBS, pH 7.6) at 4 °C. Carrageenans are sulphated linear polysaccharides extracted from red seaweeds used commonly as blockers for immunohistochemical techniques [32,33]. Primary antibody incubation was performed for 2 h at room temperature with anti-pan α1 subunit of VGCC antibody (Alomone Labs, product ACC-004) diluted 1:300 in TCT buffer, anti-TRPV5 polyclonal antibody (Alpha Diagnostic International, product CAT21-A) 10 μg/ml diluted in bidistilled water or anti-TRPV6 polyclonal antibody (Alpha Diagnostic International, product CAT11-A) 10 μg/ml diluted in bidistilled water. The anti-pan α_1 subunit of VGCC antibody is directed against an 18-residue peptide corresponding to a conserved region of the intracellular C-terminal part of the α_1 subunit, which is present in the Ca_v1 and Ca_v2 calcium channel subfamilies from all known species. Additionally, double immunostaining was performed with each of the antibodies previously described, with mouse anti-cytokeratin 7 antibody (clone OVTL 12/30, Zymed Laboratories nc.) diluted 1:100 in PBS, to confirm the trophoblastic localization of these calcium channels. After rinsing the samples with TBS, tissue sections were incubated for 1 h at room temperature with Rhodamine Red goat anti-rabbit antibody (Jackson Immunoresearch, Code Number 111-295-003) diluted 1:200 in PBS (for the anti-pan α_1 subunit of VGCC antibody) or 1:200 in bidistilled water (for the anti-TRPV5 and anti-TRPV6 antibodies). Cy2 conjugated goat anti-mouse antibody (Jackson Immunoresearch, Code Number 115-225-003) was used as secondary antibody for anti-cytokeratin 7 diluted 1:200 in PBS. Control sections were incubated with secondary antibody after incubation in TCT buffer or bidistilled water without primary antibody. Sections were viewed using a Carl Zeiss Laser Scanning Systems 510 Confocal Microscope and the Zeiss LSM 5 Image Browser.

2.7. Western blotting and densitometric analysis of blots

Isolated basal and apical purified fractions were tested for the presence of the α_1 subunit of VGCC ($n = 7$ placentas) and for the presence of TRPV5 and TRPV6 ($n = 2$ placentas) by SDS-PAGE and immunoblotting. Forty micrograms of vesicle protein together with molecular weight markers (Invitrogen BenchMark 10748-010) were loaded on a 10% SDS-polyacrylamide gel. Electrophoresis was performed at 100 V and the gel was transferred to a nitrocellulose membrane (BioRad 162-0115) for 2 h at 100 V. The nitrocellulose membrane was blocked overnight at 4 °C with 2% non-fat milk in saline buffer−Tween (in mmol/L: 1.38 NaCl, 2.7 KCl and 0.05% Tween 20), and washed in saline buffer−Tween. Membranes were incubated with primary antibody for 2 h at room temperature; anti-pan α_1 VGCC subunit polyclonal antibody (Alomone Labs, product ACC-004) was diluted 1:200 in saline buffer−Tween, anti-TRPV5 polyclonal antibody (Alpha Diagnostic International, product CAT21-A) and anti-TRPV6 polyclonal antibody (Alpha Diagnostic International, product CAT11-A) were diluted 1:400 in bidistilled water. Control antigenic peptide for each antibody was included to assess antibody specificity; for TRPV5 and TRPV6 antigenic peptides at 16 μg/μL (Alpha

Diagnostic International, product CAT21-P and CAT11-P), and for α_1 VGCC subunit antigenic peptide at 4.5 μg/μL (Alomone Labs, product ACC-004). Additionally, controls in absence of primary antibody were added in each case (only with antibody diluent). After washing with saline buffer−Tween, membranes were incubated with donkey anti-rabbit horseradish peroxidase-linked antibody (Amersham RPN 2108 NIF824) diluted 1:5000 in saline buffer−Tween for 1 h at room temperature. The final detection was done using a chemiluminiscence ECL Western Blotting Analysis System (Amersham, RPN 2106).

The anti-pan α_1 VGCC subunit polyclonal antibody developed film and its respective transferred gel were scanned using a SnapScan Touch Agfa Scanner. Protein content in lanes of the scanned images was quantified using UN-SCAN-IT gel Automated Digitizing System, version 4.1 for Windows (Silk Scientific Corporation). Densitometric values of selected lanes in the developed film were corrected by the protein densitometric quantification of the respective lane in the transferred gel. Molecular weight values for the detected bands could be obtained by scanning the molecular weight markers and using a built-in function of UN-SCAN-IT software developed for this purpose.

2.8. Data analysis

The values of relative PCa/PK were calculated using the shift in experimental reversal potential obtained when applying voltage ramps from −100 to +100 mV (40 mV/s) in the presence of $CaCl_2$ added to the Kgluconate bath solution. We used the approach described by Wollmuth et al. [34], which uses a formula derived from the Lewis equation [35] and assumes that Ca^{2+} and K^+ are the only permeant ions in the external solution and that ErevCa (that is, Erev after Ca^{2+} addition to bath) is the same as ΔErev (which requires ErevK = 0, which is the case when working in symmetrical K^+ solutions with compensation of junction potential); in this case, contribution of Na^+ (10 mmol/L in pipette and bath) to ΔErev was neglected, assuming that PK/PNa = 1, which is the case for calcium channels. The form of this equation is as follows:

$$\Delta\mathrm{Erev} = \frac{RT}{2F}\ln\left[1 + \frac{\mathrm{PCa}}{\mathrm{PK}}\frac{4\left[\mathrm{Ca}^{2+}\right]_{\mathrm{out}}}{\left[\mathrm{K}^{+}\right]_{\mathrm{out}}}\right]$$

where R is the Gas constant, T is temperature in Kelvin scale, F is Faraday's constant, Pion is the permeability of the ion, and [ion] is the concentration of the ion in the extracellular (out) or intracellular (in) solution. The values of relative PCa/PBa were calculated using the generalized Goldman−Hodgkin−Katz current equation for permeant ions at steady state (zero current):

$$I = \sum_j P_j z_j \xi \frac{\left\{[C]_j^{\mathrm{out}} - [C]_j^{\mathrm{in}}\exp(-\xi)\right\}}{1-\exp(-\xi)} = 0$$

where I is the current through the patch, P_j is the permeability of ion j, z_j is the valence of ion j, $[C]_j$ is the concentration of ion j in extracellular (out) or intracellular (in) solution, and $\xi = z\Delta VF/RT$, where ΔV is the shift in the experimental reversal potential. We thus obtained the following equation:

$$\frac{\mathrm{PCa}}{\mathrm{PBa}} = \frac{4(A) + \{(\mathrm{PCl/PBa}) \times (A) \times (\exp^{-2\xi} - \exp^{2\xi})\}}{4\{[\mathrm{Ca}]^{\mathrm{in}}\}}$$

where $A = [\mathrm{Ba}]^{\mathrm{in}} - [\mathrm{Ba}]^{\mathrm{out}}\exp^{-\xi}$. The calculation of relative PCa/PBa using the GHK current equation requires previous calculation of the value of relative PCl/PBa, which was obtained considering the contribution of Ba^{2+} and Cl^- currents (assumed to be the only current carriers in the membrane patches) to the experimental reversal potential in conditions of $BaCl_2$ pipette-to-patch gradient (condition 3 in Section 2.5). Contributions of Ba^{2+} and Cl^- currents to the average measured Erev of +32 mV ($n = 31$ independent experiments), considering the maximum range for the current reversal as 131 mV, that is the difference between the theoretical equilibrium potential for chloride ($VeqCl^- = -55$ mV) and that for Ba^{2+} ($VeqBa^{2+} = +76$ mV), were calculated as 66% and 34%, respectively, and corrected by the z values of each ion, finally obtaining a relative PCl/PBa value of 1.2.

Examination of Ba^{2+} and Cl^- currents was done measuring the currents generated when applying a 40 mV/s voltage ramp from −100 to +100 mV at $VeqCl^-$ (−55 mV) and $VeqBa^{2+}$ (+76 mV), respectively. The currents measured using these methods are denominated *total patch currents* throughout the paper.

Data were expressed as means ± SEM (standard error of the mean). Statistical differences were detected using one and two population Student's *t*-test, ANOVA or non-parametric statistics.

3. Results

The following results were obtained from a total of 99 excised patch experiments from 11 healthy term placenta purified basal membranes. Purification of basal membranes was achieved through the protocol described in Section 2, which resulted in adequate basal membrane enrichment markers and apical membrane/intracellular membrane contamination markers of the purified basal membrane fraction, as described fully in a previous paper [26].

3.1. Detection of Ca^{2+} and Ba^{2+} currents

Working with monovalent cation currents, we characterized the effect of Ca^{2+} addition to the bath solution as a strategy to detect the presence of Ca^{2+}-permeable channels. Addition of $CaCl_2$ in low millimolar concentrations (0.5−1.5 mmol/L) to the bath solution caused displacement of the reversal potential (Erev) in eight out of 11 experiments in symmetrical conditions using Kgluconate solutions (solution composition 1 in Section 2; total K concentration = 140 mmol/L), indicating Ca^{2+} conduction. The mean relative permeability ratio PCa/PK was 53.1 ± 13.7 (formula in Section 2.8), reaching values >80 in three cases. These results suggested the presence of Ca^{2+}-conducting channels in a significant proportion of our membrane patches. In order to facilitate detection of ion channel activity, we studied these Ca^{2+}-conducting channels in solutions of $BaCl_2$ (see Section 2). It was necessary to work in concentration gradient conditions (solution 3 in Section 2; in mmol/L: 40 $BaCl_2$ pipette, 0.1 $BaCl_2$ bath) to avoid disruption of liposome structure in high divalent cation concentrations and to differentiate Ba^{2+} currents from Cl^- currents which were present in 99% of our experiments. Membrane excised patches were studied using voltage ramps between −100 and +100 mV (40 mV/s), allowing for measurement of both experimental Erev and currents generated solely by Ba^{2+} ions (I_{Ba}) or Cl^- ions (I_{Cl}) at the chloride equilibrium potential ($VeqCl^- = -55$ mV) or at the Ba^{2+} equilibrium potential ($VeqBa^{2+} = +76$ mV), respectively. In $n = 31$ experiments, we observed the presence of both Ba^{2+} and Cl^- currents, evidenced by experimental Erev values situated between these ions' theoretical equilibrium potentials (mean Erev = +32 ± 3.2 mV) and also by the presence of ion channel activity at both equilibrium potentials (Fig. 1A). Addition of Ca^{2+} ($CaCl_2$ 0.5−3 mmol/L) to the bath solution caused displacement of Erev indicative of Ca^{2+} conduction ($n = 5$; Fig. 2). The total patch relative permeability ratio PCa/PBa was obtained using a GHK modified equation (see Section 2), with values ranging

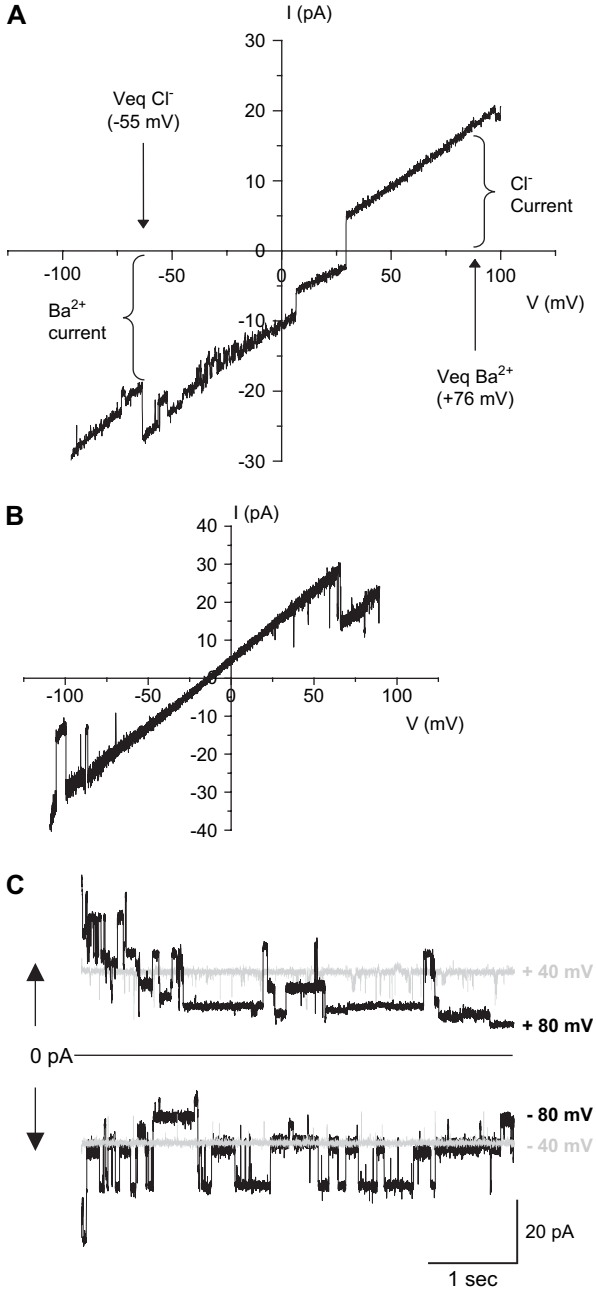

Fig. 1. Detection of barium-conducting channels and of chloride-conducting channels in excised patches. (A) Typical recording obtained using a voltage ramp in gradient conditions of $BaCl_2$ (in mmol/L: 40 $BaCl_2$ pipette, 0.1 $BaCl_2$ bath); notice channel activity at both barium and chloride Veqs, which implies the presence of barium-conducting channels and of chloride-conducting channels. This type of recording was present in 99% of our excised patches. (B and C) Recordings obtained using a voltage ramp (B) and a pulse protocol (C), as described in Section 2, in symmetrical concentrations of NMDGCl (140 mmol/L). In these conditions, it was possible to isolate a chloride channel with the classical biophysical properties of the Maxi-chloride channels: multiple substates and voltage-dependent open-probability. Arrows indicate the direction of channels openings ($n = 6$).

from 2.2 to 38.3 ($n = 5$). Addition of $CaCl_2$ in concentrations of 0.1−1.5 mmol/L both diminished I_{Ba} to 50% of control values and increased I_{Cl} up to 180% of control currents (results not shown).

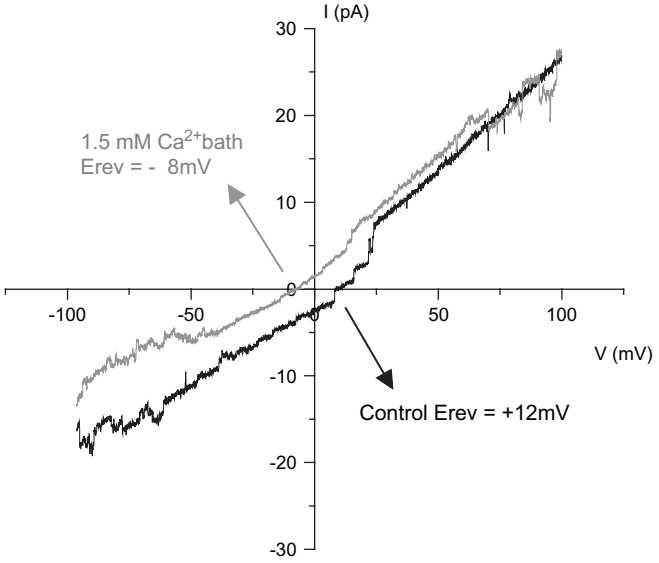

Fig. 2. Effect of millimolar calcium concentrations on Erev and total patch currents. A characteristic shift in Erev when adding millimolar concentrations of $CaCl_2$ to the bath solution in gradient conditions of $BaCl_2$ (in mmol/L: 40 $BaCl_2$ pipette, 0.1 $BaCl_2$ bath); this result reflects a high pore affinity of the recorded channels for calcium with respect to barium (detailed analysis in Section 4).

3.2. Isolation of Ba^{2+} currents using the Cl^- channel blocker DIDS followed by Ni^{2+} block of Ba^{2+} currents

Given the constant presence of Cl^- currents in our patches, we sought to obtain isolated Ba^{2+} currents by using the generalized Cl^- channel blocker DIDS. Membrane excised patches were studied under gradient conditions and voltage ramps between −100 and +100 mV, as previously described, and total patch Ba^{2+} or Cl^- currents were expressed as a ratio to control currents. Block of Cl^- currents by DIDS was most effective when working in a $BaCl_2$ concentration gradient with symmetrical (0.5 mmol/L) DIDS concentrations in pipette and bath (solution 4 in Section 2), as evidenced by an experimental Erev that shifted towards $VeqBa^{2+}$ (mean Erev = +53 ± 4.8 mV, $n = 10$, Fig. 3A). DIDS applied only to the bath solution caused a smaller shift in Erev together with equivalent reductions in Ba^{2+} and Cl^- currents (Fig. 3B); there were no statistically significant differences between 0.1 and 0.5 mmol/L DIDS concentrations ($n = 9$ and 5 for 0.1 and 0.5 mmol/L DIDS, respectively), similar results are obtained with DIDS at 1 mmol/L ($n = 2$). In these conditions, the estimated total patch relative permeability ratio PCl/PBa dropped from 1.2 (without DIDS) to 0.47 (Fig. 5).

In spite of detecting a partial block of Ba^{2+} currents when DIDS was applied to the bath solution, the experimental strategy of a $BaCl_2$ concentration gradient with symmetrical (0.5 mmol/L) DIDS concentrations in pipette and bath allowed us to work with scarce contamination of Cl^- currents. Using this strategy, we evaluated the effect of $NiCl_2$ addition to the bath solution on Ba^{2+} total patch currents and residual Cl^- total patch currents. For this purpose, we obtained the total charge generated by application of a voltage pulse using the

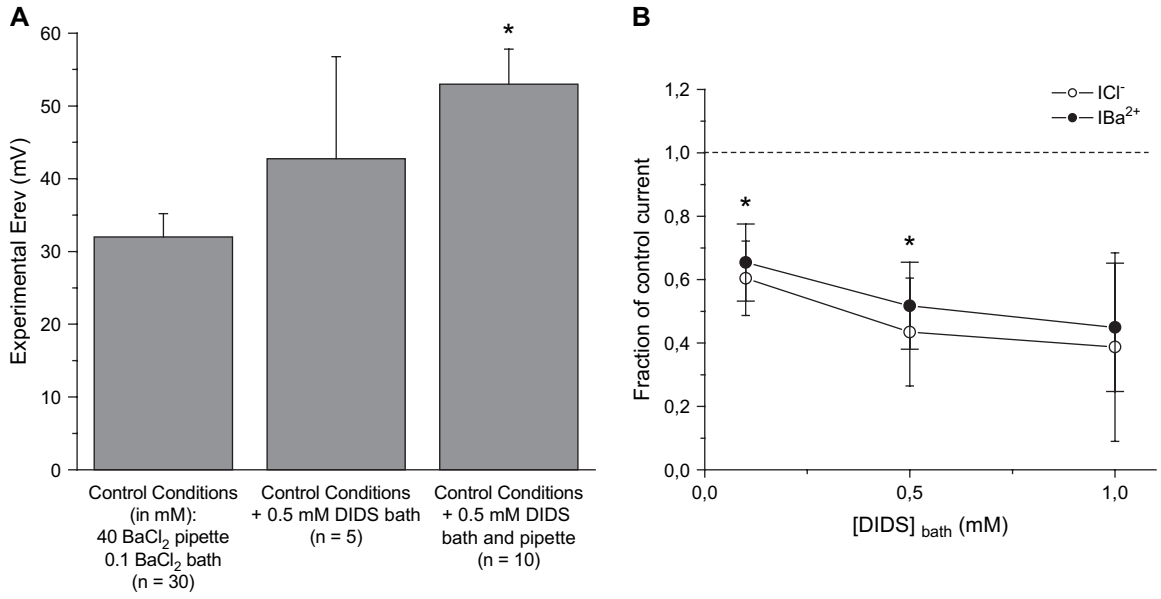

Fig. 3. Effect of chloride channel blocker DIDS on Erev and total patch currents. (A) The most efficient chloride channel blocking effect, as judged by the shift of Erev towards the barium Veq, was achieved when applying DIDS to pipette and bath ($n = 10$) as compared to control conditions (*p-value < 0.005 relative to value in control conditions, one-way ANOVA). (B) DIDS exerted blocking effects on both chloride and barium currents, reaching 50−60% block of control currents at DIDS bath concentrations of 0.5 mmol/L (*p-value < 0.05 relative to control value of 1, dotted line), similar results are obtained with DIDS at 1 mmol/L ($n = 9$, 5 and 2 for 0.1, 0.5 and 1 mmol/L DIDS, respectively). Barium total patch currents were measured at VeqCl$^-$, while chloride total patch currents were measured at VeqBa^{2+}.

Ba^{2+} and Cl^- control theoretical Veqs as holding potentials (detailed explanation in Fig. 4A and B) and analyzed the experimental reversal potentials in the presence and absence of $NiCl_2$. This allowed us to obtain the relative change in charge generated by a voltage pulse in the presence of $NiCl_2$ as compared to control conditions, and to determine the relative "weight" of Ba^{2+} and Cl^- currents in the generation of the experimental Erev; block of Ba^{2+} currents would cause a predominance of Cl^- currents and therefore a shift of Erev towards the Cl^- theoretical equilibrium potential (−55 mV). $NiCl_2$ in concentrations of 50 nmol/L to 5 mmol/L caused a 50% decrease of Ba^{2+} total patch currents and a 300% increase in Cl^- total patch currents ($n = 8$, Fig. 4C). The maximum Ba^{2+} current block was reached at 0.5 mmol/L $NiCl_2$, and addition of $NiCl_2$ up to 20 mmol/L did not increase the current block. The maximum Cl^- current increase was achieved with 10 mmol/L $NiCl_2$, with a drop to control Cl^- current values with 20 mmol/L $NiCl_2$, which could be aided by the drop in Cl^- pipette-to-patch electrochemical gradient at high $NiCl_2$ concentrations in bath solution. Experimental Erev shifted towards VeqCl$^-$ with $NiCl_2$ concentrations over 0.1 mmol/L ($n = 8$). The fact that Cl^- bath concentrations are raised when adding $NiCl_2$ to the bath causes a shift in VeqCl$^-$, as shown in Fig. 4D. This fact can diminish the absolute shift towards VeqCl$^-$ caused by a Ba^{2+}-conducting channel block, therefore underestimating the $NiCl_2$ blocking effect. To avoid this underestimation, we calculated the difference between the post-$NiCl_2$ application Erev and the corrected theoretical VeqCl$^-$ to show the blocking effect of $NiCl_2$ on Ba^{2+} currents (Fig. 4E). Using this difference, we show that $NiCl_2$ application shifts Erev to values progressively nearer to the theoretical VeqCl$^-$, only reaching it at a $NiCl_2$ concentration of 20 mmol/L with a curve that could be well fit by a second order exponential decay. The existence of two decay constants for the block of Ba^{2+} currents by $NiCl_2$ suggests two independent binding sites for this blocker, which could correspond either to two sites in a same Ba^{2+}-conducting channel or to one site in two different Ba^{2+}-conducting channels. In accordance with the described shift of Erev towards the corrected VeqCl$^-$, calculation of total patch relative permeability ratio PCl/PBa (taking into account the variations in VeqCl$^-$ at increasing $NiCl_2$ bath concentrations) showed increasing values (Fig. 5), reaching a value of 65.2 at 20 mmol/L bath $NiCl_2$ (data not shown). This result reflects the progressive loss of permeability of the membrane patch to Ba^{2+} ions, reaching very low values at high $NiCl_2$ concentrations.

3.3. Block of Ba^{2+} currents by Nifedipine and Ruthenium Red

Altogether, the previous results could be due to the presence of either one unique population or two different populations of Ba^{2+}-conducting channels. For this reason, we planned pharmacological strategies to determine the presence of one or more populations of these channels. Blockers were chosen taking into consideration the high values of relative PCa/PK obtained in the initial experiments, which suggested the presence of calcium channels in contrast to cation channels with Ca^{2+} permeability, as the latter do not present relative PCa/PCation ratios beyond 10. Among the numerous Ca^{2+} channel blockers, we chose two that could independently block populations of Ca^{2+} channels whose gene products

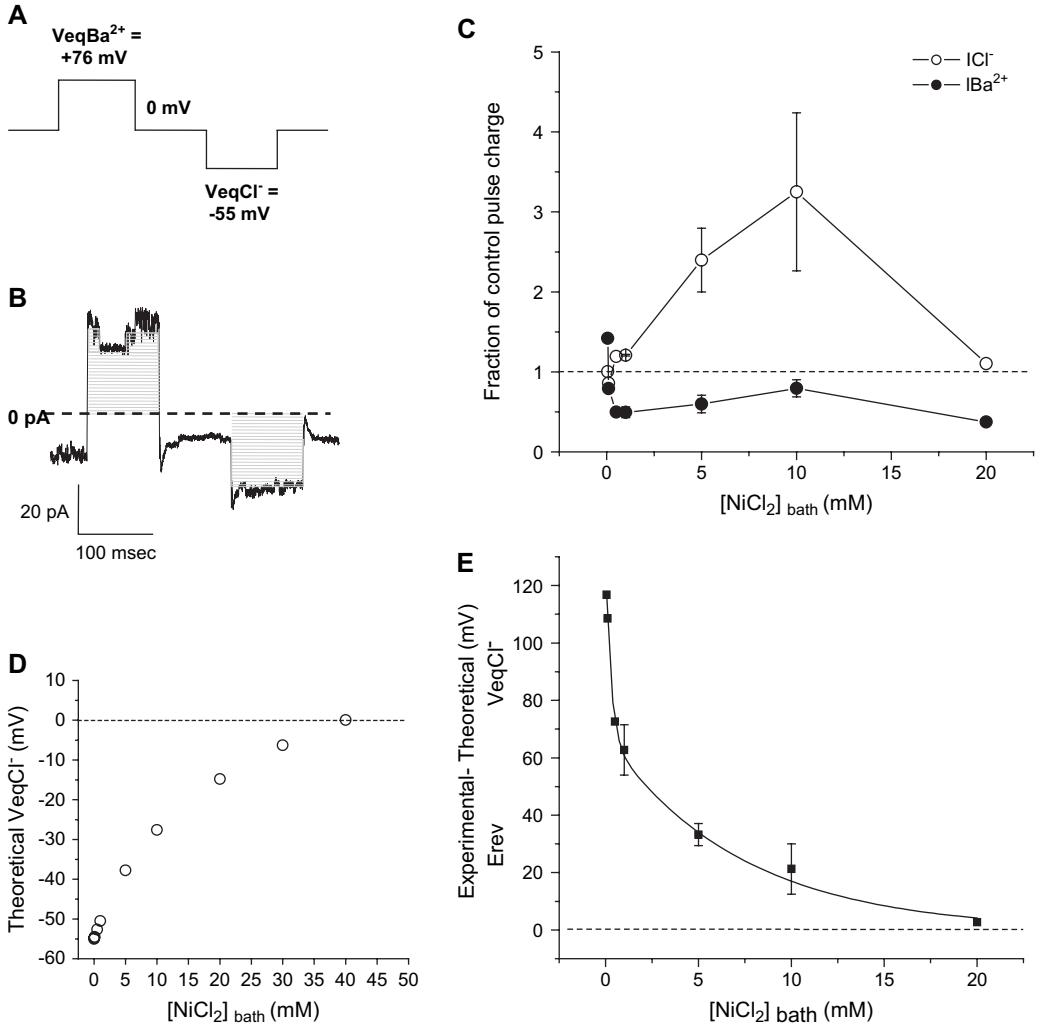

Fig. 4. Effects of nickel on Erev and pulse-generated charges. $NiCl_2$ was added to the bath solution in millimolar concentrations. Voltage pulses used to obtain pulse-generated charges are schematically shown in (A), and consist of two 100 ms pulses whose potentials were the barium and chloride Veqs separated by a 100 ms at 0 mV. A representative current recording in response to this stimulus is shown in (B). The charges were calculated using an average of 100−300 current recordings for each experiment. Charges ($q = i \times t$; where q is the charge and i is the total current during the time t) are obtained by calculating the area under the current average curve when applying either the barium Veq holding potential (to measure chloride charges) or the chloride Veq holding potential (to measure barium charges). (C) Nickel in concentrations of 0.5−20 mmol/L in bath solution reduced barium currents to 50% of control values and enhanced chloride currents to 300% of control currents ($n = 8$). (D) Addition of high $NiCl_2$ concentrations to the bath solution shifts the theoretical chloride Veq, a fact that may lead to misinterpretation of data. This phenomenon was corrected for by considering the difference between the experimental Erev and the calculated $VeqCl^-$ for every $NiCl_2$ bath concentration that was used, as shown in (E). A close to zero difference was achieved with nickel values of 20 mmol/L, meaning that the only permeant ions in these experimental conditions corresponded to chloride ions. This curve could be fit by a second order exponential decay, suggesting two binding sites for nickel ($n = 8$).

have been previously detected in human trophoblast tissue by other authors, as mentioned previously: Nifedipine (L-type VGCC blocker) and Ruthenium Red (TRPV5 and TRPV6 calcium channel blocker).

Membrane excised patches in $BaCl_2$ pipette-to-bath gradient were studied using voltage ramps to obtain total patch currents at Cl^- and Ba^{2+} theoretical equilibrium potentials, which were expressed as a ratio to control currents. Nifedipine added to the bath solution at a concentration of 1 and 5 μM reduced Ba^{2+} currents to $60 \pm 4\%$ and $48 \pm 8\%$ of control currents, respectively ($n = 5$, Fig. 6A). Nifedipine in concentrations of up to 10 μM in bath solution did not increase this block (data not shown). Surprisingly, Nifedipine also blocked Cl^- currents at all of the studied concentrations, as shown for 1 and 5 μM in Fig. 6A. Nifedipine shifted the experimental Erev towards $VeqCl^-$ in only one out of five experiments (data not shown); in the remaining experiments, Nifedipine addition did not alter the experimental Erev ($n = 3$) or shifted Erev towards $VeqBa^{2+}$ ($n = 1$). These results suggest that L-type VGCC are present in the syncytiotrophoblast basal membrane, but are probably not the only calcium channels in this membrane, as Nifedipine is unable to completely block the Ba^{2+} currents in our membrane patches.

Membrane excised patches in $BaCl_2$ pipette-to-bath gradient were studied using voltage ramps as mentioned for Nifedipine. Ruthenium Red was added to the bath solution in

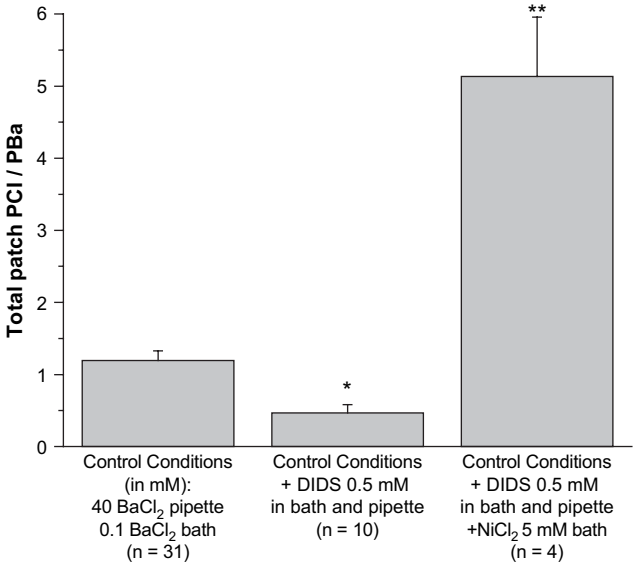

Fig. 5. Effect of nickel on total patch relative permeability ratio PCl/PBa. Nickel effect on barium currents was also analyzed by obtaining the chloride to barium relative permeability ratio using the experimental Erev, as described in the Section 2. The control relative PCl/PBa was calculated as 1.2; 0.5 mmol/L DIDS in pipette and bath reduced this ratio to 0.47. Nickel addition of 5 mmol/L to the bath solution in these conditions increased relative PCl/PBa to 5.1. *p-Value < 0.05 relative to control conditions, **p-value < 0.01 relative to control conditions.

concentrations that ranged between the IC_{50} described for TRPV5 and TRPV6 (IC_{50} TRPV5 = 111 nmol/L; IC_{50} TRPV6 = 9.5 μmol/L). The 50% block of total Ba^{2+} current was achieved at concentration of 555 nmol/L ($n = 3$; Fig. 6B) and Ruthenium Red blocked Ba^{2+} currents up to a 37% of control currents at 18 μM (data not shown). There were no statistically significant differences in the percentual block by 555 nmol/L and 9.5 μmol/L Ruthenium Red; however, addition of 1 μmol/L Nifedipine to the bath solution after block by 9.5 μmol/L Ruthenium Red diminished the Ba^{2+} current an additional 30% in one experiment (47% of control Ba^{2+} current before Nifedipine, 18% of control Ba^{2+} current after Nifedipine; Fig. 6B). Ruthenium Red also blocked Cl^- currents at all of the applied concentrations. The blocking effect of Ba^{2+} currents by Ruthenium Red at concentrations lower than those needed to block L-type voltage-dependent calcium channels (L-type calcium channel $IC_{50} = 25.4$ μmol/L) suggests the presence of other Ba^{2+}-conducting channels with high sensitivity to this blocker, such as TRPV channels or non-L-type VGCC (P/Q-type or N-type).

3.4. Immunohistochemical detection of VGCC and TRPV5–TRPV6 channels in syncytiotrophoblast basal and apical membranes

We pursued the detection of α_1 subunit of VGCC using a polyclonal antibody against a conserved segment in the α_1 subunit of the Ca_v1 and Ca_v2 subfamilies, and of TRPV5 and TRPV6 channels using corresponding polyclonal antibodies. As can be seen in Fig. 7A, D and G for each antibody, respectively, transverse sections of placental villi show a predominant stain for all three antibodies in the periphery, probably corresponding to the syncytiotrophoblast sheet. Morphologically, the fluorescent immunostaining seems not to be present in intracellular membranes, but is clearly distinguished in the syncytiotrophoblast basal and apical membranes, with a more intense stain in the latter. Additionally, double immunostaining was performed to confirm the trophoblastic localization of these channels in microvillous and basal syncytiotrophoblast membranes. As shown in Fig. 7B, E and H for anti-cytokeratin 7 plus anti-α_1 subunit of VGCC, anti-TRPV5 and anti-TRPV6 antibodies, respectively, the

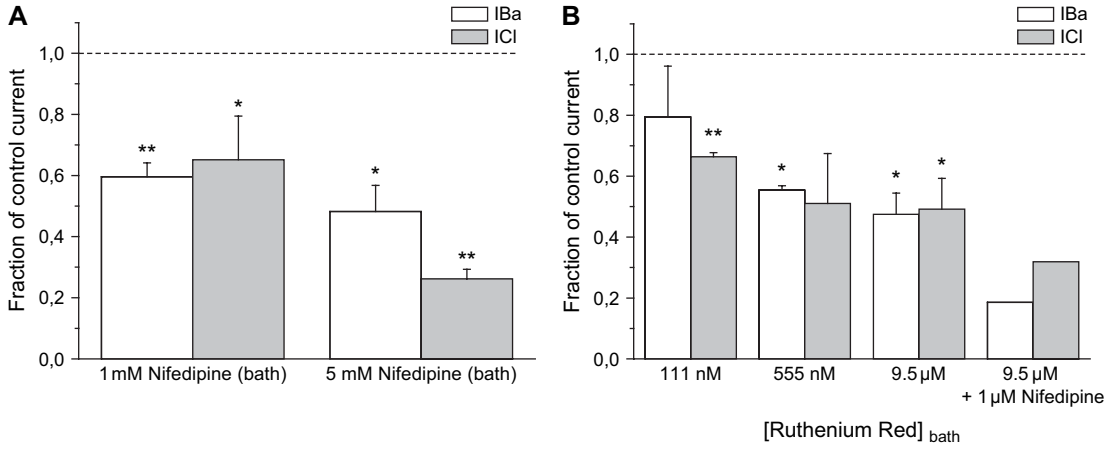

Fig. 6. Block of barium currents by Nifedipine and Ruthenium Red. (A) Nifedipine caused a significant decrease in barium currents with respect to control values, which were measured at the chloride Veq; surprisingly, Nifedipine also reduced chloride currents, which were measured at the barium Veq in voltage ramps ($n = 5$). (B) Ruthenium Red caused a significant decrease in barium currents measured at the chloride Veq in voltage ramps, reaching 50% of control current at 555 nmol/L (which corresponds to TRPV6 IC50, $n = 3$). Notice that addition of 1 μmol/L Nifedipine to the bath solution after addition of 9.5 μmol/L Ruthenium Red caused an additional barium current block of 29%, suggesting simultaneous presence of calcium channels with different pharmacological sensitivity. Chloride currents measured at the barium Veq in voltage ramps were unexpectedly and significantly blocked by both Nifedipine ($n = 5$) and Ruthenium Red ($n = 3$). *p-Value < 0.05 relative to control value of 1, **p-value < 0.01 relative to control value of 1.

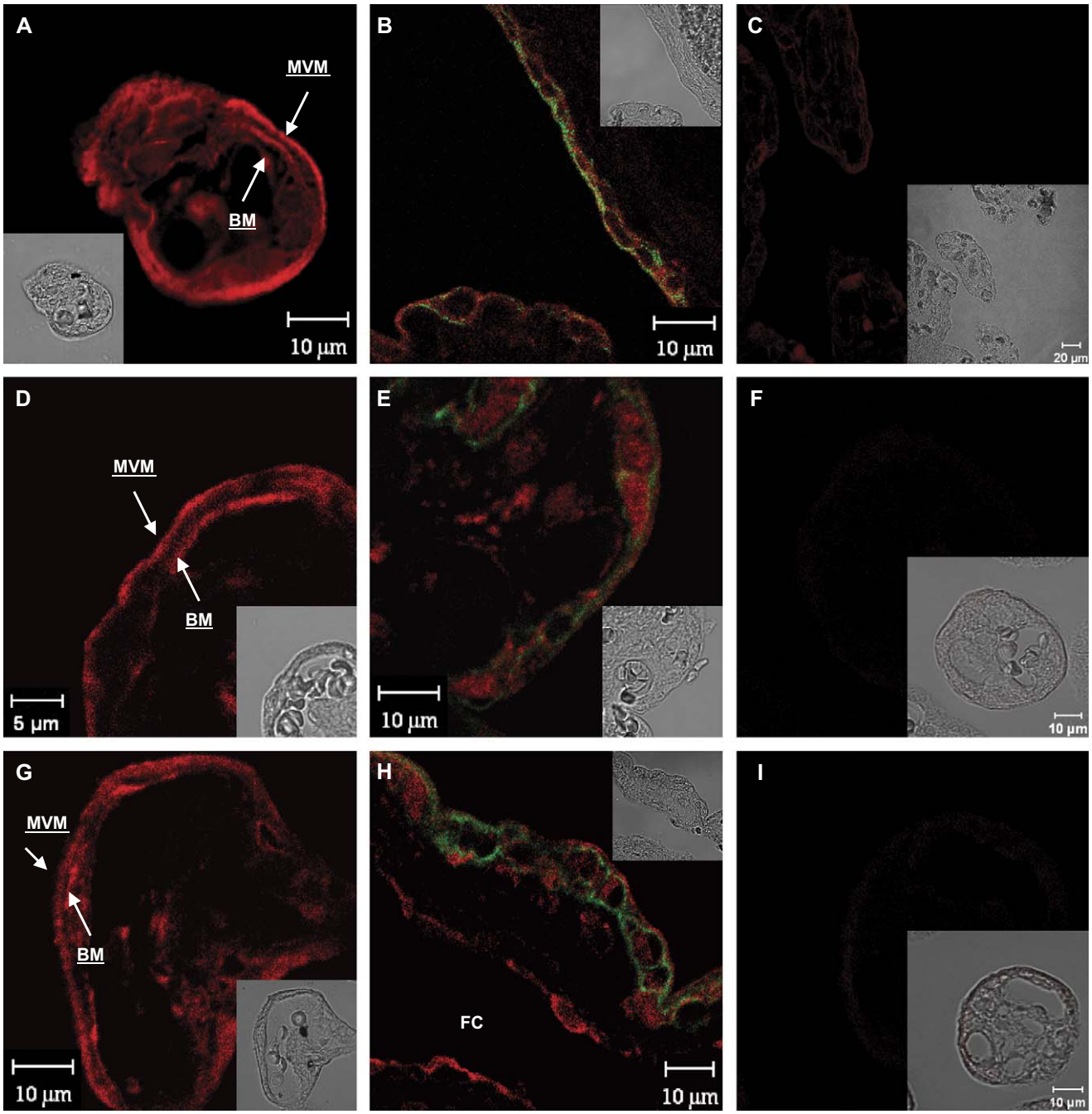

Fig. 7. Detection of voltage-gated calcium channels (VGCC) and TRPV5−TRPV6 channels in apical and basal membranes of normal term human placentas. Confocal fluorescence micrographs with their respective transmitted light micrographs (insets) of immunohistochemical sections of placental villous tissue using primary antibodies against α_1 subunit of VGCC (A), TRPV5 (D) and TRPV6 (G). C, F, I, respective controls using only secondary antibody (without primary antibody). B, E, and H show double immunostaining of anti-cytokeratin 7 antibody with α_1 subunit of VGCC, TRPV5 and TRPV6, respectively. MVM = microvillous (apical) membrane, BM = basal membrane, FC = fetal capillary.

cytoskeletal protein cytokeratin 7 is detected only in the periphery of villous tissue, clearly staining the syncytiotrophoblast. The three types of calcium channels were detected in some areas that correspond to apical and basal syncytiotrophoblast membranes. TRPV5 and TRPV6, but not the α_1 subunit of VGCC, also show a cytoplasmatic pattern of staining. Control sections show an almost imperceptible stain (Fig. 7C, F and I).

3.5. Western blot detection of VGCC, TRPV5 and TRPV6 in basal and apical syncytiotrophoblast purified membranes

Western blots using a polyclonal antibody against the α_1 subunit of VGCC of the Ca_v1 and Ca_v2 subfamilies (α_1 subunit of VGCC) were pursued using samples of paired basal and apical purified fractions for a total of seven placentas,

whose purified fractions were used in electrophysiological experiments. Fig. 8A shows a representative Western blot with bands corresponding to the molecular weight of the α_1 subunit of VGCC in both basal (BM) and apical (MVM) membrane purified fractions, together with their respective control with antigen peptide and control without primary antibody, none of the controls showing a specific band. Fig. 8B shows a representative Western blot (inset) with bands corresponding to the molecular weight of the α_1 subunit of VGCC in both BM and MVM purified fractions, together with bands corresponding to the molecular weight of placental alkaline phosphatase (PLAP). The PLAP band was much more marked in the apical purified fraction than in the basal purified fraction, as can be seen in the corresponding densitometric analysis; the basal PLAP band corresponds to less than 10% of the sum of apical and basal PLAP densitometrically quantified bands, while the basal α_1 subunit of VGCC band corresponds to more than 30% of the sum of apical and basal α_1 subunit of VGCC densitometrically quantified bands.

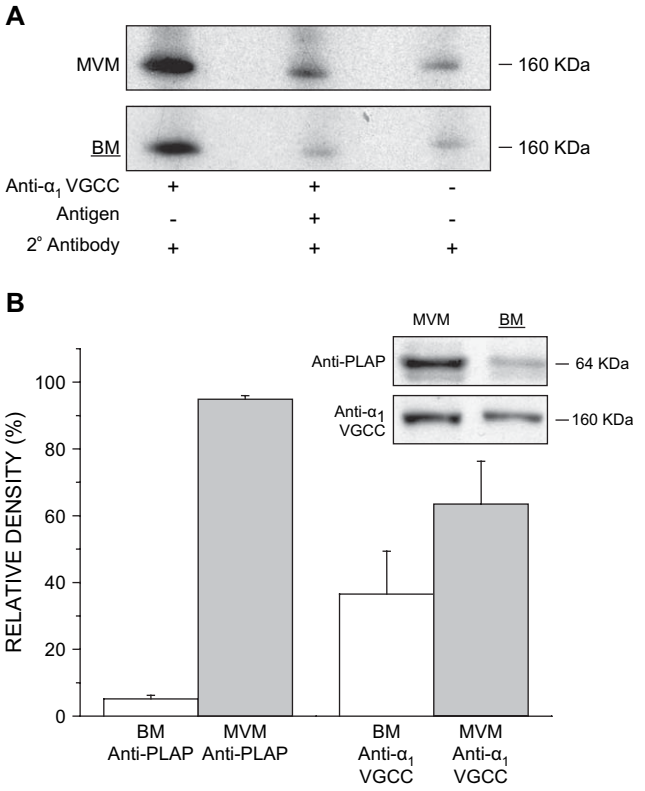

Fig. 8. (A) Western blotting for α_1 subunit of VGCC in purified apical (MVM) and basal (BM) membranes. Peptide antigen control and control without primary antibody are also shown. α_1 subunit of VGCC shows a clear band in each, apical and basal membranes. Consequently with this result, there is a weak band shown for antigenic peptide control whose signal is almost completely removed, thus, verifying the antibody specificity. Control without primary antibody shows a weak band which can be compared equally to the antigenic peptide control signal, inferring that this is a non-specific signal from the secondary antibody. (B) Western blotting and densitometric analysis for placental alkaline phosphatase (PLAP) and α_1 subunit of VGCC in purified apical and basal membranes. Densitometric analysis of developed film corrected by gel protein quantification (as explained in Section 2.7). Values are expressed as a percentage of the sum of the corrected PLAP or α_1 subunit of VGCC in either purified apical or purified basal membrane ($n = 7$; mean ± SEM), such that (BM anti-PLAP + MVM anti-PLAP) = 100% and (BM anti-α_1 subunit of VGCC + MVM anti-α_1 subunit of VGCC) = 100%. As can be seen, less than 10% of PLAP is contained in the BM purified fraction, while more than 30% of α_1 subunit of VGCC is present in this purified fraction, revealing that at least 20% of total α_1 subunit of VGCC is contained in purified BM and does not correspond to contamination from MVM purified fraction. Inset, representative Western Blot of MVM and BM purified fractions from the same placenta. Molecular weight of bands was obtained using densitometric analysis of bands in developed films, as explained in Section 2.

Western blots using polyclonal antibodies against TRPV5 and TRPV6 were pursued using samples of paired basal and apical purified fractions for a total of three placentas. Fig. 9 shows a representative Western blot with bands corresponding to the molecular weights of TRPV5 and TRPV6 in both basal and apical membrane purified fractions, with their respective antigenic peptide control. TRPV5 and TRPV6 show a strong band in both of the purified syncytiotrophoblast membranes, and each of them is almost completely eliminated with the preadsorption treatment with their respective antigenic peptide, similar to those obtained in the control without primary antibodies (data not shown).

4. Discussion

In the present study we report, for the first time, detection of Ca^{2+}-conducting channel activity in human syncytiotrophoblast basal membrane through reconstitution of highly purified basal membrane fractions in an artificial lipidic system suitable for patch-clamp electrophysiological recordings. These channels had the following electrophysiological characteristics: PCa/PK values ranging between 12 and 100, high PCa/PBa values, block by low micromolar concentrations of Ca^{2+} ions, block by micromolar concentrations of Ni^{2+} ions, and block by Nifedipine and Ruthenium Red. The channels were present in 100% of the membrane patches studied in $BaCl_2$ solutions, accompanied by chloride channels in 99% of the patches. The ion channel activity genuinely pertains to the basal syncytiotrophoblast membrane, as its high prevalence does not correlate with the detected quantity of cross-contamination of BM with MVM, mitochondrial membranes [26] or non-syncytial plasma membranes [27].

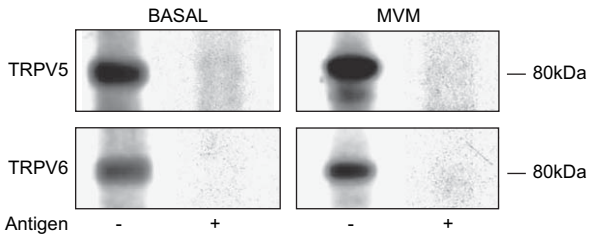

Fig. 9. Western blotting for TRPV5 and TRPV6 channels in basal and apical syncytiotrophoblast purified membranes with their respective antigenic peptide control. Representative blot shows, at expected molecular weight, the presence of TRPV5 and TRPV6 channels in both basal and apical purified membrane fractions. This specific result was confirmed by preadsorption of the primary antibody with the corresponding antigenic peptide.

The value of PCa/PK in solutions of K^+ gluconate with micromolar concentrations of Ca^{2+} added to the bath solution displayed variable values, including values comparable to PCa/PK of non-selective cation channels with low selectivity for Ca^{2+} ions (PCa/PK = PCa/PNa $\leq$ 10; $n = 3$), PCa/PK of non-selective cation channels with high selectivity for Ca^{2+} ions (PCa/PK = PCa/PNa $\approx$ 100; $n = 3$) [22], and intermediate values ($n = 2$). These findings are compatible with the presence of members of the superfamily of TRP channels with different Ca^{2+} to monovalent cation relative permeabilities in the basal syncytiotrophoblast membrane (TRPC and TRPV family members).

The value of PCa/PBa in $BaCl_2$ gradients also displayed variable values, comparable to the PCa/PBa of VGCC (PCa/PBa < 10; $n = 2$) [36] and to the PCa/PBa of TRPV5 and TRPV6 (PCa/PBa $\approx$ 17−19; $n = 3$) [37]. These results are compatible with the presence of these two types of Ca^{2+} channels in the studied membranes. There are presently insufficient data in the literature concerning Ba^{2+} permeability in TRPC channels, so comparison with our experimental values is not possible.

Ca^{2+} added in concentrations ranging between 0.1 and 3 mmol/L in the bath solution blocked Ba^{2+} currents up to 50%. This block could be due to high affinity of Ca^{2+} for the channel's pore, a characteristic present in both voltage-dependent calcium channels [18] and TRP channels with high permeability to Ca^{2+} (TRPV5 and TRPV6) [38,39], hence this result is compatible with the functional presence of any of these two types of channels in our reconstituted purified basal membranes. Ni^{2+} added in concentrations ranging between 0.5 and 5 mmol/L in the bath solution also blocked Ba^{2+} currents up to 50%. Concentrations of 0.1 mmol/L were unable to block these currents efficiently; in contrast, Ca^{2+} was able to achieve a maximum effect at this concentration, suggesting a higher affinity of the channels for Ca^{2+} than for Ni^{2+}. On the other hand, Ni^{2+} has been studied as a blocker of Ca^{2+} channels for decades, with blocker concentrations for VGCC usually in the millimolar range [40], and has also been shown to inhibit Ca^{2+} currents through TRPV5 in the micromolar range [41].

The changes in total patch relative PCl/PBa when adding Ni^{2+} to the bath solution may be due to changes in total patch permeability to Cl^- ions, total patch permeability to Ba^{2+} ions, or simultaneous changes in both variables. The addition of DIDS to both pipette and patch caused a decrease in total patch relative PCl/PBa from 1.2 to 0.47, which considering the decrease in I_{Cl} and I_{Ba} caused by DIDS, was interpreted as due to a fall in the relative permeability to Cl^-. Following this same line of analysis, the consistent rise in total patch relative PCl/PBa when adding Ni^{2+} to the bath solution could be interpreted as a rise in the relative permeability to Cl^-, a fall in the relative permeability to Ba^{2+}, or both simultaneous phenomena. The rise in I_{Cl} and the fall in I_{Ba} suggest a combination of the two phenomena at least up to $NiCl_2$ concentrations of 10 mmol/L.

$NiCl_2$ concentrations that reached 5 mmol/L in bath solution did not block Ba^{2+} currents over 50%, which is an expected behavior for VGCC, as mentioned. Erev closely resembled the corrected $VeqCl^-$ when adding 20 mmol/L $NiCl_2$, evidencing an almost complete block of Ba^{2+} currents which is compatible with the millimolar Ni^{2+} block of VGCC and the micromolar Ni^{2+} block of TRPC and TRPV [41,42]. The data of the difference between Erev and $VeqCl^-$ vs. $NiCl_2$ bath concentration were well fit by a second order exponential decay, which may be due to the presence of two Ni^{2+} binding sites in different molecules, as previously discussed in the results. However, it must be emphasized that Ni^{2+} block of Ca^{2+} channels usually follows complex kinetics and studies have proposed two separate sites for its blocking action in N-type and T-type VGCC [40], a possibility which must not be discarded in our results.

Usual values for Nifedipine block of L-type Ca^{2+} channels are in the micromolar range [43,44]. Addition of Nifedipine in concentrations between 1 and 10 μmol/L to the bath solution reduced Ba^{2+} currents to 50−60% of control values, which suggests the presence of L-type VGCC; there is presently no evidence that supports block of other Ba^{2+}-permeable channels by Nifedipine in these concentrations. The remaining Ba^{2+} current could be due either to the presence of dihydropyridine-insensitive channels or to unfavorable conditions for Nifedipine block of L-type channels (i.e. low probability of open or inactivated channel states). The lack of shift of Erev was not an expected result if the only effect of Nifedipine addition was block of Ba^{2+} currents. Since in our experimental conditions Erev depends on the balance between Ba^{2+} and Cl^- currents, the only explanation for a lack of Erev shift is an equivalent fall in both currents when adding Nifedipine. Indeed, Cl^- currents are reduced when adding Nifedipine to the bath. As there are no reports of dihydropyridine block of anion channels in the literature, a remaining possibility is the existence of a functional interaction between the recorded Ca^{2+} and Cl^- channels that is kept in the conditions of purified membrane reconstitution, such that Nifedipine block of Ca^{2+} channels affects conductance and/or gating kinetics of the accompanying Cl^- channel.

Ruthenium Red is an organometallic dye that acts as an inhibitor of a wide range of Ca^{2+}-binding proteins, including ion channels such as ryanodine receptors, Ca^{2+}-activated K^+ channels, VGCC and TRP channels [45]. Despite its widespread cation channel blocking action, differences in blocking concentrations allow its use to aid in the functional identification of Ca^{2+} channels; a particular case is that of the TRPV subfamily, as TRPC and TRPM channels are not sensitive to Ruthenium Red [46]. We have obtained block of Ba^{2+} currents by Ruthenium Red using concentrations much lower than those of the IC_{50} blocking concentrations for TRPV6 (9.5 μmol/L), compatible with the presence of both TRPV5 and TRPV6 channels. Addition of 1 μmol/L Nifedipine further raised the block of 9.5 μmol/L Ruthenium Red, supporting the presence of functional L-type VGCC and TRPV channels in our purified basal membranes.

Immunohistochemical studies that show the presence of Ca^{2+}-permeable channels in the syncytiotrophoblast plasma membrane using human trophoblast villous tissue have

presently only been done by Clarson et al., who detected TRPC3 and TRPC4 in both basal and apical membranes [17]. Our immunohistochemical studies clearly show the presence of VGCC, TRPV5 and TRPV6 channels in the syncytiotrophoblast villous layer, as can be seen in the double immunostaining experiments with anti-cytokeratin 7. This is an antibody that gives a cytoplasmatic pattern of staining and thus, it was used to confirm the trophoblastic localization of the Ca^{2+} channels' antibodies used in some areas. The anti-cytokeratin 7 immunostaining results allowed us to demonstrate that the stain from Ca^{2+} channels antibodies used was for the most part in the syncytiotrophoblast. The presence of α_1 subunits of VGCC, TRPV5 and TRPV6 both in the basal and apical purified syncytiotrophoblast membranes is in accordance with the immunohistochemical results and represents a molecular correlation of our electrophysiological findings in reconstituted purified basal membranes.

Ba^{2+}-conducting activity was a constant feature in our recordings, which is by itself an important result that reflects the high density of Ca^{2+} channels in our purified basal membrane. Another interesting and unexpected result was the constant association of Cl^- currents to our Ba^{2+} currents; only one out of 76 excised patch experiments showed the presence of a solitary Ba^{2+} current (evidenced by an Erev that closely resembled VeqBa^{2+}, data not shown), and no experiments showed Cl^- currents on their own. One possible explanation is the presence of a high density of Ca^{2+}-dependent Cl^- channels, as we never worked with Ca^{2+}-free solutions and Ca^{2+} concentrations in de-ionized water can be in the low range of micromolar values, which can be enough to activate these types of currents [47]. Another possibility is the existence of a functional and/or topographical relationship between the detected calcium and Cl^- channels, which is an interesting alternative that must be explored. Although there are a few reports of block of Cl^- channels by Ni^{2+} and Ruthenium Red [48,49], the constant block of Cl^- currents by the Ca^{2+} channel blockers (including Nifedipine) is a result that suggests a functional relationship between Ca^{2+} and Cl^- channels. Likewise, DIDS block of Ba^{2+} currents could either be due to a direct action of this classical Cl^- channel blocker on Ca^{2+} channels, as is the case for Ryanodine Receptors and TRPC [50], or due to the mentioned functional relationship.

The results of our study provide functional and immunohistological evidence for the presence of VGCC and TRPV5−TRPV6 channels in the basal membrane of human syncytiotrophoblast. Results of other studies published in the literature to date are both in favor of and against the presence of functional VGCC in this plasma membrane, as mentioned in the introduction. An important contribution to the evidence against the presence of these channels is the study performed by Cronier et al., who did not find VGCC-type currents when using patch-clamp recordings in whole cell configuration in primary villous trophoblastic cell culture [13]. On the other hand, our results are in agreement with those of other authors, who have detected the presence of mRNA for VGCC, TRPV5 and TRPV6 in trophoblasts from term placentas (see Belkacemi et al. [51] for a review of recent literature).

The role of Ca^{2+} channels in the basolateral membrane of transport epithelia has generally been associated to functions other than transcellular transport of this ion [52], due to the energy requirements of Ca^{2+} absorption: Ca^{2+} enters the apical epithelial membrane following a favorable electrochemical gradient, travels through the cytoplasm bound to Ca^{2+}-binding proteins, and exits the basolateral membrane against the electrochemical gradient. This transport includes a passive apical step, which can be achieved by Ca^{2+}-permeable channels or Ca^{2+} passive transporters, and an active basolateral step, which can be achieved by active transporters (ATP-coupled or gradient-coupled) [53]; Ca^{2+} channels cannot participate in this last step, so their presence in epithelial basal/basolateral membranes must respond to other necessities (i.e. syncytiotrophoblast hormone secretion). Nevertheless, Ca^{2+} channels in the basal syncytiotrophoblast membrane could indirectly participate in transcellular Ca^{2+} transport through regulatory mechanisms that involve PTH and PTHrP [54]. Studies have suggested the participation of PTHrP in placental Ca^{2+} transfer and trophoblast growth and differentiation [55]. In a study by Farrugia et al. [56], both PTH and PTHrP enhanced Ca^{2+} efflux from basal, not apical, purified human syncytiotrophoblast membrane vesicles. PTH and PTHrP have been shown to exert their actions through modulation of L-type VGCC in multiple cell types [57]. The presence of L-type Ca^{2+} channels in syncytiotrophoblast membranes is then an expected finding given the relevance of these hormones in placental function. Such analysis is at the moment not possible for TRP channels. Their role in the basal syncytiotrophoblast membrane must continue to be studied from a molecular and functional point of view.

Overall, current evidence for the role of Ca^{2+} as a second messenger in the human placental syncytiotrophoblast demands for the functional study of plasma membrane Ca^{2+} channels in this epithelium. Our work contributes to the functional detection and molecular characterization of these channels, and we believe it is a good starting point to explore the regulation of Ca^{2+} as a second messenger by fetal factors.

References

[1] Hochberg Z, Bick T, Perlman R, Lahav M, Barzilai D. The modulation of placental lactogen secretion by calcium: studies with cultured human term trophoblast. Mol Cell Endocrinol 1984;37:359−62.

[2] Zeitler P, Murphy E, Handwerger S. Arachidonic acid stimulates 45calcium efflux and hPL release in isolated trophoblast cells. Life Sci 1986;38:99−107.

[3] Hochberg Z, Perlman R, Bick T. Interrelated calcium ion and cyclic AMP inhibition of placental lactogen secretion by cultured human term trophoblast. Acta Endocrinol (Copenh) 1987;114:68−73.

[4] Petraglia F, Lim AT, Vale W. Adenosine 3′,5′-monophosphate, prostaglandins, and epinephrine stimulate the secretion of immunoreactive gonadotropin-releasing hormone from cultured human placental cells. J Clin Endocrinol Metab 1987;65:1020−5.

[5] Belisle S, Petit A, Bellabarba D, Escher E, Lehoux JG, Gallo-Payet N. Ca2+, but not membrane lipid hydrolysis, mediates human chorionic gonadotropin production by luteinizing hormone-releasing hormone in human term placenta. J Clin Endocrinol Metab 1989;69:117−21.

[6] Petit A, Gallo-Payet N, Vaillancourt C, Bellabarba D, Lehoux JG, Belisle S. A role for extracellular calcium in the regulation of placental

lactogen release by angiotensin-II and dopamine in human term trophoblastic cells. J Clin Endocrinol Metab 1993;77:670−6.

[7] Shi CZ, Zhuang LZ. Norepinephrine regulates human chorionic gonadotrophin production by first trimester trophoblast tissue in vitro. Placenta 1993;14:683−93.

[8] Shi CZ, Zhuang LZ. Stimulatory effect of norepinephrine on progesterone production by human first trimester placenta explants in vitro. Life Sci 1993;52:1657−65.

[9] Meuris S, Polliotti B, Robyn C, Lebrun P. Ca2+ entry through L-type voltage-sensitive Ca2+ channels stimulates the release of human chorionic gonadotrophin and placental lactogen by placental explants. Biochim Biophys Acta 1994;1220:101−6.

[10] Polliotti B, Lebrun P, Robyn C, Meuris S. The release of human chorionic gonadotrophin and placental lactogen by placental explants can be stimulated by Ca2+ entry through a Na(+)−Ca2+ exchange process. Placenta 1994;15:477−85.

[11] Robidoux J, Simoneau L, Masse A, Lafond J. Activation of L-type calcium channels induces corticotropin-releasing factor secretion from human placental trophoblasts. J Clin Endocrinol Metab 2000;85:3356−64.

[12] Moreau R, Simoneau L, Lafond J. Characteristics of calcium uptake by BeWo cells, a human trophoblast cell line. Placenta 2001;22:768−75.

[13] Cronier L, Dubut A, Malassine A. Effects of endothelin on villous trophoblast differentiation and free intracellular calcium. Trophoblast Res 1999;13:69−86.

[14] Niger C, Malassine A, Cronier L. Calcium channels activated by endothelin-1 in human trophoblast. J Physiol 2004;561:449−58.

[15] Moreau R, Hamel A, Daoud G, Simoneau L, Lafond J. Expression of calcium channels along the differentiation of cultured trophoblast cells from human term placenta. Biol Reprod 2002;67:1473−9.

[16] Moreau R, Daoud G, Bernatchez R, Simoneau L, Masse A, Lafond J. Calcium uptake and calcium transporter expression by trophoblast cells from human term placenta. Biochim Biophys Acta 1564;2002:325−32.

[17] Clarson LH, Roberts VH, Hamark B, Elliott AC, Powell T. Store-operated Ca2+ entry in first trimester and term human placenta. J Physiol 2003;550:515−28.

[18] Sather WA, McCleskey EW. Permeation and selectivity in calcium channels. Annu Rev Physiol 2003;65:133−59.

[19] Catterall WA, Striessnig J, Snutch TP, Perez-Reyes E. International Union of Pharmacology. XL. Compendium of voltage-gated ion channels: calcium channels. Pharmacol Rev 2003;55:579−81.

[20] Tsien RW. Calcium channels in excitable cell membranes. Annu Rev Physiol 1983;45:341−58.

[21] Montell C, Birnbaumer L, Flockerzi V, Bindels RJ, Bruford EA, Caterina MJ, et al. A unified nomenclature for the superfamily of TRP cation channels. Mol Cell 2002;9:229−31.

[22] Clapham DE, Montell C, Schultz G, Julius D. International Union of Pharmacology. XLIII. Compendium of voltage-gated ion channels: transient receptor potential channels. Pharmacol Rev 2003;55:591−6.

[23] Llanos P, Henriquez M, Riquelme G. A low conductance, non-selective cation channel from human placenta. Placenta 2002;23:184−91.

[24] Gonzalez-Perrett S, Kim K, Ibarra C, Damiano AE, Zotta E, Batelli M, et al. Polycystin-2, the protein mutated in autosomal dominant polycystic kidney disease (ADPKD), is a Ca2+-permeable nonselective cation channel. Proc Natl Acad Sci U S A 2001;98:1182−7.

[25] Lafond J, Leclerc M, Brunette MG. Characterization of calcium transport by basal plasma membranes from human placental syncytiotrophoblast. J Cell Physiol 1991;148:17−23.

[26] Jimenez V, Henriquez M, Llanos P, Riquelme G. Isolation and purification of human placental plasma membranes from normal and preeclamptic pregnancies: a comparative study. Placenta 2004;25:422−37.

[27] Illsley NP, Wang ZQ, Gray A, Sellers MC, Jacobs MM. Simultaneous preparation of paired, syncytial, microvillous and basal membranes from human placenta. Biochim Biophys Acta 1990;1029:218−26.

[28] Riquelme G, Stutzin A, Barros LF, Liberona JL. A chloride channel from human placenta reconstituted into giant liposomes. Am J Obstet Gynecol 1995;173:733−8.

[29] Gasnier F, Rousson R, Lerme F, Vaganay E, Louisot P, Gateau-Roesch O. Use of Percoll gradients for isolation of human placenta mitochondria suitable for investigating outer membrane proteins. Anal Biochem 1993;212:173−8.

[30] Riquelme G, Lopez E, Garcia SL, Ferragut JA, Gonzalez RJ. Giant liposomes: a model system in which to obtain patch-clamp recordings of ionic channels. Biochemistry 1990;29:11215−22.

[31] Hamill OP, Marty A, Neher E, Sakmann B, Sigworth FJ. Improved patch-clamp techniques for high-resolution current recording from cells and cell-free membrane patches. Pflugers Arch 1981;391:85−100.

[32] Trius A, Sebranek JG. Carrageenans and their use in meat products. Crit Rev Food Sci Nutr 1996;36:69−85.

[33] Renaud-Young M, Gallin WJ. In the first extracellular domain of E-cadherin, heterophilic interactions, but not the conserved His−Ala−Val motif, are required for adhesion. J Biol Chem 2002;277:39609−16.

[34] Jatzke C, Watanabe J, Wollmuth LP. Voltage and concentration dependence of Ca(2+) permeability in recombinant glutamate receptor subtypes. J Physiol 2002;538:25−39.

[35] Lewis CA. Ion-concentration dependence of the reversal potential and the single channel conductance of ion channels at the frog neuromuscular junction. J Physiol 1979;286:417−45.

[36] Pizarro G, Fitts R, Uribe I, Rios E. The voltage sensor of excitation−contraction coupling in skeletal muscle. Ion dependence and selectivity. J Gen Physiol 1989;94:405−28.

[37] Vennekens R, Hoenderop JG, Prenen J, Stuiver M, Willems PH, Droogmans G, et al. Permeation and gating properties of the novel epithelial Ca(2+) channel. J Biol Chem 2000;275:3963−9.

[38] den Dekker E, Hoenderop JG, Nilius B, Bindels RJ. The epithelial calcium channels, TRPV5 & TRPV6: from identification towards regulation. Cell Calcium 2003;33:497−507.

[39] Jean K, Bernatchez G, Klein H, Garneau L, Sauve R, Parent L. Role of aspartate residues in Ca(2+) affinity and permeation of the distal ECaC1. Am J Physiol Cell Physiol 2002;282:C665−72.

[40] Zamponi GW, Bourinet E, Snutch TP. Nickel block of a family of neuronal calcium channels: subtype- and subunit-dependent action at multiple sites. J Membr Biol 1996;151:77−90.

[41] Peng JB, Chen XZ, Berger UV, Vassilev PM, Tsukaguchi H, Brown EM, et al. Molecular cloning and characterization of a channel-like transporter mediating intestinal calcium absorption. J Biol Chem 1999;274:22739−46.

[42] Wang J, Shimoda LA, Sylvester JT. Capacitative calcium entry and TRPC channel proteins are expressed in rat distal pulmonary arterial smooth muscle. Am J Physiol Lung Cell Mol Physiol 2004;286:L848−58.

[43] Hille B. Ionic channels of excitable membranes. Sunderland, MA: Sinauer Associates; 1992.

[44] Charnet P, Ouadid H, Richard S, Nargeot J. Electrophysiological analysis of the action of nifedipine and nicardipine on myocardial fibers. Fundam Clin Pharmacol 1987;1:413−31.

[45] Cibulsky SM, Sather WA. Block by ruthenium red of cloned neuronal voltage-gated calcium channels. J Pharmacol Exp Ther 1999;289:1447−53.

[46] Peng JB, Brown EM, Hediger MA. Epithelial Ca2+ entry channels: transcellular Ca2+ transport and beyond. J Physiol 2003;551:729−40.

[47] Qu Z, Hartzell HC. Anion permeation in Ca(2+)-activated Cl(−) channels. J Gen Physiol 2000;116:825−44.

[48] Gincel D, Zaid H, Shoshan-Barmatz V. Calcium binding and translocation by the voltage-dependent anion channel: a possible regulatory mechanism in mitochondrial function. Biochem J 2001;358:147−55.

[49] Matchkov VV, Aalkjaer C, Nilsson H. A cyclic GMP-dependent calcium-activated chloride current in smooth-muscle cells from rat mesenteric resistance arteries. J Gen Physiol 2004;123:121−34.

[50] Hill AP, Sitsapesan R. DIDS modifies the conductance, gating, and inactivation mechanisms of the cardiac ryanodine receptor. Biophys J 2002;82:3037−47.

[51] Belkacemi L, Bedard I, Simoneau L, Lafond J. Calcium channels, transporters and exchangers in placenta: a review. Cell Calcium 2005;37:1−8.

[52] Bush KT, Stuart RO, Li SH, Moura LA, Sharp AH, Ross CA, et al. Epithelial inositol 1,4,5-trisphosphate receptors. Multiplicity of localization, solubility, and isoforms. J Biol Chem 1994;269:23694−9.

[53] Stulc J. Placental transfer of inorganic ions and water. Physiol Rev 1997;77:805−36.

[54] Laramee M, Simoneau L, Lafond J. Phospholipase C axis is the preferential pathway leading to PKC activation following PTH or PTHrP stimulation in human term placenta. Life Sci 2002;72:215−25.

[55] Clemens TL, Cormier S, Eichinger A, Endlich K, Fiaschi-Taesch N, Fischer E, et al. Parathyroid hormone-related protein and its receptors: nuclear functions and roles in the renal and cardiovascular systems, the placental trophoblasts and the pancreatic islets. Br J Pharmacol 2001; 134:1113−36.

[56] Farrugia W, de Gooyer T, Rice GE, Moseley JM, Wlodek ME. Parathyroid hormone(1−34) and parathyroid hormone-related protein(1−34) stimulate calcium release from human syncytiotrophoblast basal membranes via a common receptor. J Endocrinol 2000;166:689−95.

[57] Lalonde M, Li B, Kline L, Pang P, Karpinski E. Modulation of L-type Ca2+ channels in UMR 106 cells by parathyroid hormone-related protein. Life Sci 2001;70:503−15.

[58] Long O, Clarson LH. The effect of Ca^{2+}-permeable channel blockers on human chorionic gonadotrophin (hCG) secretion by villous fragments from term placentas. J Physiol 2002;S220:539.